

Reconfigurable chirality with achiral excitonic materials in the strong-coupling regime

P. Elli Stamatopoulou,¹ Sotiris Droulias,² Guillermo P. Acuna,³ N. Asger Mortensen,^{1,4} and Christos Tserkezis¹

¹*Center for Nano Optics, University of Southern Denmark, Campusvej 55, DK-5230 Odense M, Denmark*

²*Department of Digital Systems, University of Piraeus, GR-18534, Piraeus, Greece*

³*Department of Physics, University of Fribourg, Chemin du Musée 3, Fribourg CH-1700, Switzerland*

⁴*Danish Institute for Advanced Study, University of Southern Denmark, Campusvej 55, DK-5230 Odense M, Denmark*

(Dated: November 16, 2022)

We introduce and theoretically analyze the concept of manipulating optical chirality via strong coupling of the optical modes of chiral nanostructures with excitonic transitions in molecular layers or semiconductors. With chirality being omnipresent in chemistry and biomedicine, and highly desirable for technological applications related to efficient light manipulation, the design of nanophotonic architectures that sense the handedness of molecules or generate the desired light polarization in an externally controllable manner is of major interdisciplinary importance. Here we propose that such capabilities can be provided by the mode splitting resulting from polaritonic hybridization. Starting with an object with well-known chiroptical response—here, for a proof of concept, a chiral sphere—we show that strong coupling with a nearby excitonic material generates two distinct frequency regions that retain the object’s chirality density and handedness, which manifest most clearly through anticrossings in circular-dichroism or differential-scattering dispersion diagrams. These windows can be controlled by the intrinsic properties of the excitonic layer and the strength of the interaction, enabling thus the post-fabrication manipulation of optical chirality. Our findings are further verified via simulations of the circular dichroism of a realistic chiral architecture, namely a helical assembly of plasmonic nanospheres embedded in a resonant matrix.

I. INTRODUCTION

Chirality is encountered widely in nature, describing, in its most broad definition, the possibility of an object not being superimposable onto its mirror image. It is a common characteristic of biomolecules, massively determining their chemical function and interactions. For instance, chiral assemblies have been shown to regulate autophagy—the mechanism responsible for recycling unnecessary components within cells—whose abnormal regulation is associated with diseases such as cancer and diabetes [1]. In the pharmaceutical and food industry opposite handedness is oftentimes the factor that distinguishes between harmful and beneficial substances [2, 3]. It is, therefore, not to wonder why sensing and controlling chirality has remained the subject of intense study for decades, with optical characterization techniques attracting particular attention [4]. Besides biomedical interest, chiral structures have attracted the attention of the photonic—particularly plasmonic [5]—community, due to their ability to distinguish between left-/right-handed circularly polarized (L/RCP) light, rendering them ideal platforms for the study of optical activity and the chiroptical effects associated with it [6]. They have been proposed as building blocks for metamaterials for the generation of superchiral light [7], negative refraction [8] and as broadband circular polarizers [9]. Control of chiral matter–light interactions at the quantum level has also received significant attention for applications in quantum information technologies [10, 11].

The origin of optical activity in photonic systems can be attributed to different manifestations of chirality. Small metal clusters have been shown to exhibit intrinsic chirality, owing to the asymmetric arrangement of achiral

adsorbates on their surfaces [12]. Moreover, nanoparticles (NPs)—most commonly metallic—arranged in specific geometries can demonstrate optical chirality stemming from their structural characteristics [13]. Finally, a chiral response can also be induced externally, either by means of chiral inclusions in achiral metasurfaces [14] or by external magnetic fields [15]. For example, magnetic circular dichroism (MCD) describes a special case of magnetically induced chirality, where an otherwise achiral object becomes optically active in the presence of a static magnetic field, as observed in gyroelectric media [16, 17].

Chirality is typically quantified by measuring the circular dichroism (CD) and the differential scattering (DS) of a sample [18], referring to the different absorption and scattering, respectively, of LCP and RCP light that it undergoes. However, conventional CD spectroscopy is restricted to a narrow range of applications, due to the general weakness of the corresponding signals in natural chiral materials [19]. Several approaches for enhancing the sensitivity of the measurements have been proposed, from superchiral fields [20] and metamaterials [21], to resonant single NPs and NP arrays [22–26] or self-assemblies [27]. Plasmon-induced chirality has been demonstrated both theoretically [28] and experimentally [29, 30] through interaction of chiral molecules with achiral metallic NPs, which are famous for strongly enhancing the local electromagnetic (EM) field. At the same time, considerable effort has also focused on high-index dielectric NPs and metasurfaces [31–34].

Here we propose an efficient route for manipulating the response of chiral structures, by means of reconfiguring their photonic environment. Excitonic materials that sustain resonant modes stemming from excitonic transitions at the atomic level have already been

proposed and explored as a means to control the optical response in conventional plasmonic assemblies. In recent works, the marriage of plasmonic NPs with J -aggregates of organic molecules or with two-dimensional (2D) transition-metal dichalcogenides (TMDs) that exhibit excitonic transitions, operating in the strong coupling regime, has paved the way for a new era of flexible and multifunctional platforms for modern nanophotonic applications [35]. Such composite architectures give rise to hybrid states, termed exciton polaritons or plexcitons, that combine the properties of both light and matter [36]. In addition to plexcitons, high-index dielectrics are more recently being considered as alternative environments for excitonic strong coupling, potentially as a way to surpass the hurdle of high Ohmic losses dominating metals, or to design novel polaritons with a magnetic character [37–39]. Strong coupling of a chiral excitonic material with an achiral resonator (e.g. a plasmonic NP) has already been shown to generate wide anticrossings in experimentally measured CD spectra [40]. Here we theoretically explore chiral structures whose CD and DS is rendered reconfigurable via the addition of an achiral excitonic environment. Such a configuration has been studied in the case of two coupled metallic nanorods [41], but it is much more general and can be observed in any chiral system, as we discuss below. As a proof of principle, we first probe a simple, analytically solvable configuration, that of a non-dispersive high-index dielectric sphere with intrinsic chirality, covered with an excitonic layer. Then we proceed to a system with structural chirality, namely silver (Ag) NPs in a helical arrangement. We observe the distinct behaviour of the system when operating in the strong coupling regime, dominated by large spectral anticrossings not only in absorption spectra but also in CD, showcasing thus the engineering possibilities offered by these hybrid systems.

II. RESULTS AND DISCUSSION

The chirality of a system is encoded within its constitutive relations, that relate the electric field \mathbf{E} and magnetic induction \mathbf{B} to the displacement field \mathbf{D} and the magnetic field \mathbf{H} via the introduction of the Pasteur parameter κ [42],

$$\mathbf{D} = \varepsilon\varepsilon_0\mathbf{E} + i(\kappa/c)\mathbf{H} \quad (1a)$$

$$\mathbf{B} = \mu\mu_0\mathbf{H} - i(\kappa/c)\mathbf{E}, \quad (1b)$$

which typically takes complex values. In eqn (1), ε and μ denote the relative permittivity and permeability of the chiral medium respectively, ε_0 and μ_0 the corresponding vacuum values, and $c = 1/\sqrt{\varepsilon_0\mu_0}$ is the speed of light in vacuum. The eigenmodes of an infinite isotropic such medium are L/RCP (+/-) waves that propagate with refractive indices $n_{\pm} = n_c \pm \kappa$ respectively, where $(n_+ + n_-)/2 = n_c = \sqrt{\varepsilon\mu}$ is the average (background) refractive index. The Pasteur parameter κ describes cou-

pling between electric and magnetic field components, and is generally related to the $\mathbf{D} \cdot \mathbf{B}$ product.

As a means to quantify the chiral properties of an EM field, the local chirality density is employed, defined as [43]

$$C = -\frac{\omega}{2} \text{Im}\{\mathbf{D}^* \cdot \mathbf{B}\}, \quad (2)$$

where ω is the angular frequency of light. From eqn (2) it is clear that the chirality density is associated with parallel electric and magnetic components that are properly phase shifted. Regarding the sign of chirality density, it is interesting to note that it is preserved when the duality symmetry of the EM field is fulfilled [24, 44].

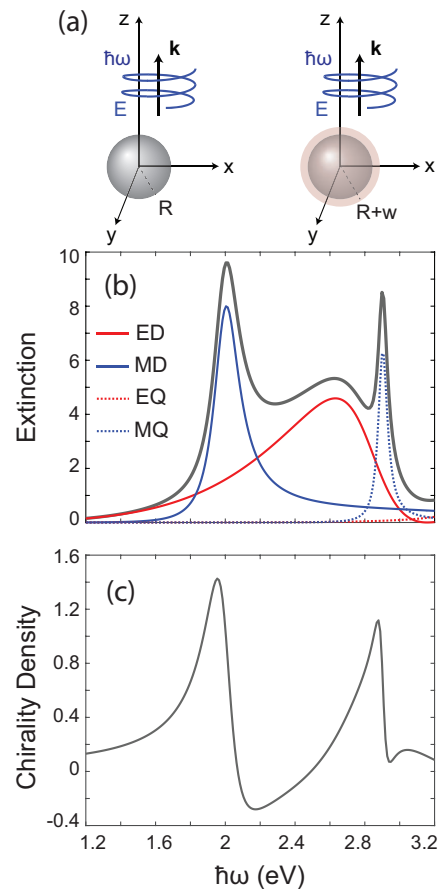


FIG. 1. (a) Sketch of a chiral sphere illuminated by a circularly polarized wave of energy $\hbar\omega$ and wavevector \mathbf{k} (left), and the corresponding exciton-covered NP studied in Figs. 2 and 3. (b) Extinction cross section (grey curve), normalized to the geometrical cross section πR^2 of an achiral sphere with radius $R = 85$ nm and dielectric function $\varepsilon = 12.1 + 0.001i$, excited by an LCP wave. The contribution from electric/magnetic dipolar/quadrupolar Mie modes is shown by red/blue solid/dotted lines. (c) Chirality density of the same NP integrated over its volume and normalized to the corresponding value of chirality density in the bulk of the medium (see ESI).

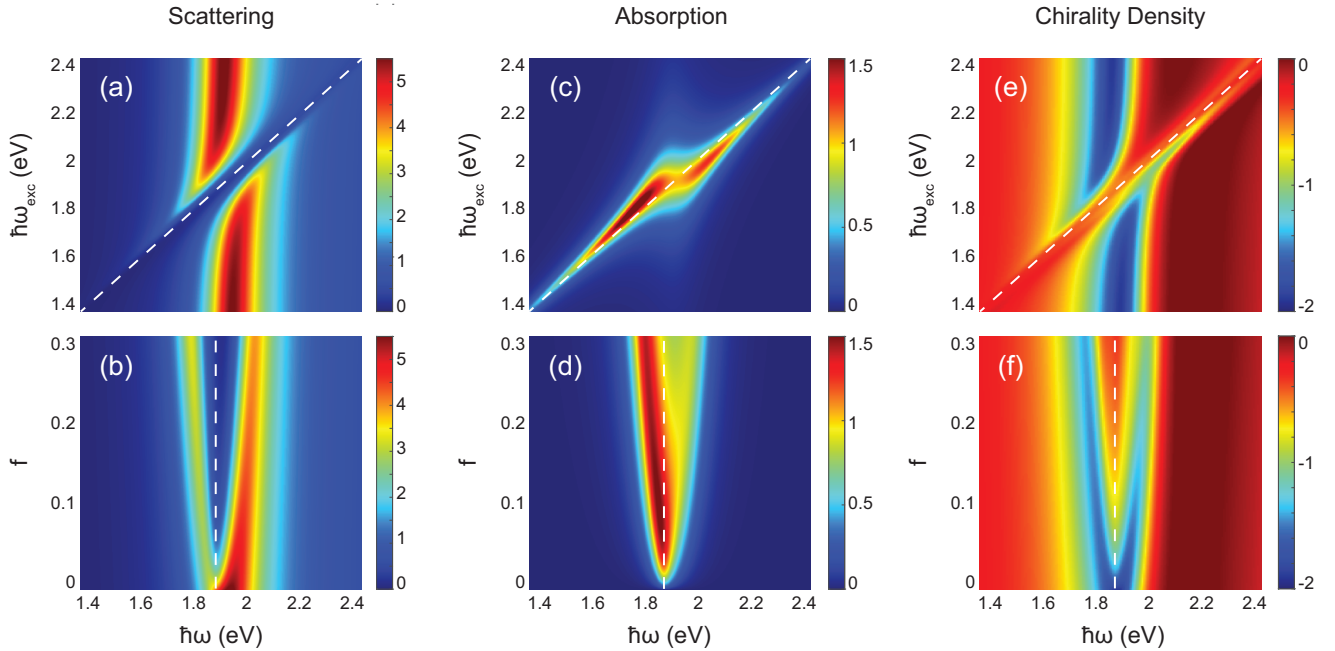


FIG. 2. (a-b) Scattering and (c-d) absorption cross sections (normalized to the geometrical cross section) and (e-f) chirality density spectra (normalized to the corresponding bulk values) of the achiral sphere of Fig. 1(b) coated with an excitonic shell of thickness $w = 20$ nm as a function of (a,c,e) the excitonic transition energy $\hbar\omega_{\text{exc}}$ (for $f = 0.2$) and (b,d,f) the excitonic oscillator strength f (for $\hbar\omega_{\text{exc}} = 1.88$ eV). For the excitonic material we use the parameters $\varepsilon_b = 3$ and $\hbar\gamma_{\text{exc}} = 0.05$ eV. Here (and in Figs. 3 and 5), superimposed dashed white lines serve as guides to the eye for tracing the energy of the excitonic resonance. In all panels the NP is excited by LCP light.

To explore the effect of an excitonic environment on the chirality response of optically active matter, it is important to first understand the impact of the excitonic coating on its resonant features, i.e. the overlapping electric and magnetic modes. To this end, and in order to maintain complexity at a minimum, we first study in Fig. 1(b) the optical response of a spherical high-index, achiral ($\kappa = 0$) NP, 85 nm in radius, characterized by a constant permittivity $\varepsilon = 12.1 + 0.001i$ and permeability $\mu = 1$, illuminated by a plane EM wave [see left-hand sketch in Fig. 1(a)]. Due to the very small imaginary part of the permittivity, the absorption in the NP is negligible and light is mostly scattered [45]. Rigorous analytic Mie theory [46] in Fig. 1(b) predicts a magnetic dipolar (MD) mode at around 2 eV, a broad electric dipolar mode (ED) centered at about 2.6 eV, and a sharp magnetic quadrupolar mode (MQ) at 2.9 eV, whereas higher-order modes (e.g. the electric quadrupole, EQ) are negligible in the energy window we operate. The electric and magnetic modes exhibit a significant spectral overlap in certain energy windows. We therefore expect local chirality density hotspots at these energies, at the points that host parallel electric and magnetic components, not only in the space surrounding the sphere, but also in its volume, since the scattered fields and the ones developing inside the NP are resonant at similar energies; the Mie coefficients describing each, exhibit poles at the same eigenfrequencies. Indeed, the chirality density spectrum integrated over the

volume of the NP (see ESI for the analytic expression) in Fig. 1(c) reveals local extrema close to the energies where magnetic and electric modes intersect. We stress, however, that this overlap should be taken as an indication, rather than a condition for high chirality density. After all, extinction is mostly due to the fields scattered in the environment of the sphere, rather than fields in its volume where the chirality density is evaluated.

Once the excitonic component is introduced, here as a concentric shell of thickness w [see right-hand sketch in Fig. 1(a)] to retain the existence of exact analytic solutions, the system features two types of resonant modes, the electromagnetic Mie resonances and the matter-like excitonic resonances [37]. The dielectric function of the excitonic material is for simplicity given by the Lorentz model

$$\varepsilon(\omega) = \varepsilon_b - \frac{f\omega_{\text{exc}}^2}{\omega^2 - \omega_{\text{exc}}^2 + i\gamma_{\text{exc}}\omega}, \quad (3)$$

where ε_b is the background permittivity, ω_{exc} is the frequency of the excitonic transition (described in the model as a harmonic oscillator), f is the oscillator strength, and γ_{exc} the damping rate. When the resonant features of each constituent (Mie-resonant and excitonic) are tuned to the same frequency, they couple in a manner analogous to the classical problem of two coupled harmonic oscillators. If the interaction is strong enough, i.e. in the strong-coupling regime, the energy states of the Lorentz oscillator and the optical modes are tied together, leading

to the emergence of two hybrid light–matter resonances, identified in dispersion spectra by the avoided crossing or anticrossing of the modes, also referred to as *Rabi splitting* due to its analogy to quantum optics [36, 47].

Fig. 2 shows the normalized (to the geometrical cross section) scattering and absorption cross section of the composite NP (achiral NP and excitonic shell) for varying parameters of the Lorentz oscillator, as well as the corresponding chirality density of the coupled system. We note here that we chose to couple the exciton resonance to the MD mode of the particle, since it exhibits a well-defined linewidth, but similar coupling can be achieved with the ED and the higher order modes of the particle. Therefore, since the MD mode is the one primarily coupling to the excitonic transition, it is deliberately the only one taken into account in the Mie expansions in Figs. 2(a)–(d), in order to understand the resulting modification of the optical response of the particle on a fundamental level. In practice, however, there is a low contribution of the ED mode in the 1.4 – 2.4 eV energy window, i.e. the low-energy tail of the red line in Fig. 1(b), and a weak coupling also occurs between the exciton and the ED mode. The anticrossing trend between the MD mode and the excitonic resonance, as the latter is shifted in energy, illustrated in the scattering spectrum of Fig. 2(a), reveals that the system is possibly strongly coupled. The width of the split serves as a qualitative measure of the coupling strength and can be tuned via the oscillator strength of the excitonic transition [see Fig. 2(b)]. In Fig. 2(c) and (d) we show the effect of the excitonic shell on the absorption spectrum for varying excitonic transition energy and oscillator strength, respectively. The pattern observed in Fig. 2(c) where the mode splitting is not clearly discernible is sometimes referred to as *induced transparency* [48]. Examination of the strong coupling criteria, however, reveals that the system indeed operates in the strong coupling regime (see ESI). The chirality density, only taking the dipolar modes (MD, ED) of the coupled structure into account, follows the anticrossing behaviour of the scattering spectrum [see Fig. 2(e) and (f)]. Since the change in chirality density is significant, we expect a highly tunable CD and DS signal once we introduce chiral properties to the dielectric core of the structure.

We next explore the impact of the excitonic environment on an optically active configuration. Fig. 3(a) and (c) show the CD and DS of the same coated dielectric NP, now with a chiral core characterized by $\kappa = 0.001$. This particular value of the chirality parameter serves two purposes: on the one hand, it is small enough to ensure that the electric and magnetic modes will be coupled but will otherwise remain unaffected, and on the other hand it is real-valued, leading to a typically very weak CD signal of the core alone (see ESI). In passing, here we define the DS and CD signal as [18]

$$\text{CD} = \sigma_{\text{abs}}^{\text{R}} - \sigma_{\text{abs}}^{\text{L}} \quad (4a)$$

$$\text{DS} = \sigma_{\text{scat}}^{\text{R}} - \sigma_{\text{scat}}^{\text{L}}, \quad (4b)$$

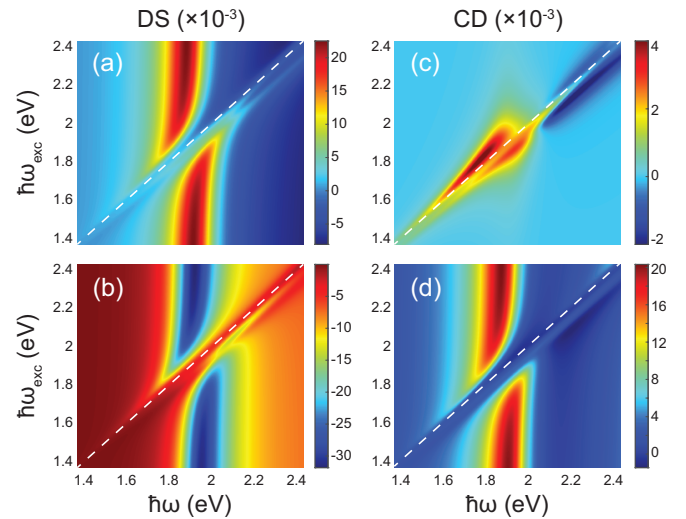


FIG. 3. Photon versus exciton energy colour map of the (a-b) DS and (c-d) CD corresponding to the same coated NP as in Fig. 2, here with a chiral core described by the Pasteur parameter $\kappa = 0.001$ (panels a and c) and $\kappa = 0.001i$ (panels b and d).

where $\sigma_{\text{abs/scat}}^{\text{R/L}}$ is the absorption/scattering cross section corresponding to an R/LCP incident light wave normalized to the geometrical cross section, analytic expressions for which can be found in several textbooks for optically active media [45].

As already mentioned, for a weak real-valued chiral parameter κ one would perhaps expect a negligible CD signal. On the contrary, Fig. 3(c) proves that the presence of the excitonic material has led to a significant CD component, even comparable to the DS component as shown in Fig. 3(a). The reason is that chirality lifts the degeneracy of the Mie modes between excitation with LCP and RCP waves, as is already evident in the DS calculations. As a result, and despite the absence of absorbing chiral regions, asymmetric absorption takes place in the achiral regions of the combined shell-sphere system, mainly the excitonic shell, thus leading to nonzero CD signal. This observation is in accord with theoretical predictions of nonvanishing CD signals in achiral metasurfaces with chiral inclusions characterized by entirely real κ [14]. Additionally, this is the reason why, eventually, the CD signal inherits the behaviour of the absorption in the achiral particle, as presented in Fig. 2(c). We note, that —in contrast with Fig. 2— what we plot in all panels of Fig. 3 is the *total* optical response of the structure, including higher order electric and magnetic modes, since the MD mode, albeit the primary radiating channel, is not the only mode that is supported in the operating energy window. On the other hand, the effect of the excitonic layer on the already significant DS component is the splitting of the resonant spectral feature. Similar to the achiral structure, those effects can become more prominent as we tune the oscillator strength of the

excitonic material (see ESI).

Figs. 3(b) and (d) show the effect of the excitonic shell on the chiral properties of an NP with imaginary $\kappa = 0.001i$, in which case the uncoated NP already exhibits a significant CD signal (see ESI). Here, the DS spectrum exhibits, as before, an anticrossing trend as in the case of real-valued κ . The CD spectrum, however, attains a completely different behavior. What we observe in this case is the splitting of the spectral feature as the two components are detuned, similarly to the DS spectrum. When κ is imaginary-valued, the contribution of the chiral material regions to asymmetric absorption dominates over that in the achiral regions. In this case, CD locally behaves as $CD(\mathbf{r}) \propto \text{Im}(\kappa)C(\mathbf{r})$ [24], and therefore inherits the anticrossing trend of the chirality density C , as seen in Fig. 2(e).

We have established so far that excitonic materials can be successfully employed to reconfigure the chirality response of a system by means of either amplifying the intensity of the measured signal, or adding new spectral features, even in the least sophisticated structures. Among the numerous nanostructures that have been shown in recent years to demonstrate strong structural optical chirality, metallic-NP helices, whose optical activity is encoded in the geometry of the system rather than the optical parameters, attract considerable interest [27, 49, 50]. Due to their intense plasmonic near fields, they significantly enhance chiroptical effects, while also offering unique control and tunability capabilities provided by DNA-origami assembling [51, 52], which has evolved into the main nanofabrication technique for such systems. Recently, we analyzed how such plasmonic NP helices can be employed as efficient templates for the evaluation of quantum-informed models for plasmonics [53]; here we employ the same architecture as a realistic example of the reconfigurable chirality discussed above.

In what follows, we consider Ag nanospheres (described by the experimental permittivity of Johnson and Christy [54]) of radius $R = 5$ nm, a size that lies within the limits of what can realistically be supported by DNA origami [55]. Each helix contains 7 particles, arranged around the z axis, and revolving by steps of 30° , so that 7 particles constitute one full revolution about z , as shown in the schematics of Fig. 4(a). The vertical center-to-center distance of the spheres along z is $2R$. In this arrangement, the distances between nearest-neighbour NPs are really small, nearly touching, thus ensuring intense plasmonic interactions, which are expected to lead to collective plasmonic chain modes at frequencies ω_c , that propagate along the direction of the field polarization [56], thus generating characteristic spectral features that are sensitive to both the NP arrangement and the incident polarization [53]. For more details about the simulations, see ESI.

Fig. 4 shows the absorption cross section and CD spectra for propagation along the helix axis (z), as sketched in (a). In panel (b) we show the absorption spectra (normalized to the geometric cross section of an individual

NP) in the absence of an excitonic shell for L/RCP polarized light (orange/green curve), together with the spectrum of the excitonic matrix alone (grey dashed curve); the matrix is an ellipsoid just enclosing the entire helix (long axis 30 nm, short axis 17.5 nm) described by the generic Lorentzian of eqn (3) with $\varepsilon_b = 1$, $f = 0.02$ and $\hbar\gamma_{\text{exc}} = 0.052$ eV, while in this particular spectrum we choose $\hbar\omega_{\text{exc}} = 2.4$ eV. The absorption spectrum is characterized by two low-energy resonances, close in energy, labeled as peaks A and B, that correspond to chain plasmons at energies $\hbar\omega_c$, emerging from the interaction of individual spheres along the direction of the incident po-

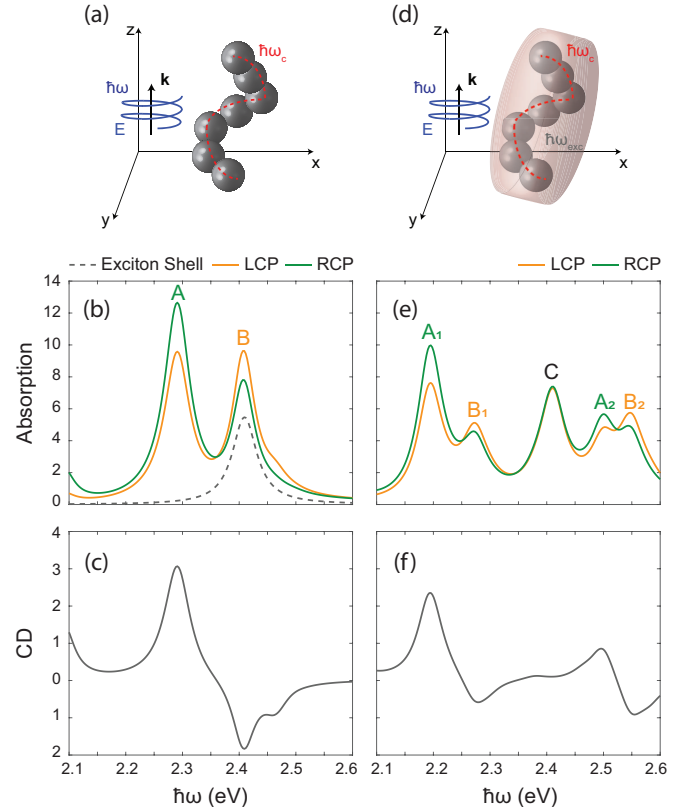


FIG. 4. (a) Schematic of an Ag-NP helix: 7 nanospheres, of radius $R = 5$ nm each, revolve around a hypothetical supporting pillar along the z axis, with steps of 30° , separated by a vertical distance $2R$ along z . The helix is illuminated by circularly polarized light of frequency ω propagating along z , and excites a collective chain mode at frequency ω_c . (b) Normalized (to the geometrical cross section of a single sphere) absorption cross sections for the 7-NP Ag helix of (a), for RCP (green curve) and LCP (orange curve) incident light propagating along the helix axis, in the absence of an excitonic shell. The grey dashed spectrum is that of the excitonic shell alone, with transition energy $\hbar\omega_{\text{exc}} = 2.4$ eV. (c) CD spectrum of the uncoupled helix of (a). (d) Schematic of the helix of (a), now embedded in an excitonic matrix with a transition at ω_{exc} , modelled as an ellipsoid described by the permittivity of eqn (3). (e) Same absorption spectra as in (b), with the excitonic layer present (with $\hbar\omega_{\text{exc}} = 2.4$ eV), and (f) the corresponding CD spectrum.

larization; since the incident light contains both x and y electric-field components, small sub-chains are excited along both directions, with slightly smaller energies because of the different effective number of chains in each direction [53]. Fig. 4 shows a different preference in absorption at the energies of the two resonances; as indicated by the color of the labels, resonance A absorbs RCP light more efficiently than LCP, and the opposite occurs for resonance B. The scattering spectra of these helices are characterized by similar features, only much weaker in amplitude, since such small plasmonic NPs are dominated by absorption. Such modes have an electric and magnetic character simultaneously, since they emerge from the circulation of the electric dipolar plasmonic modes of individual NPs, leading thus naturally to strong chiroptical activity.

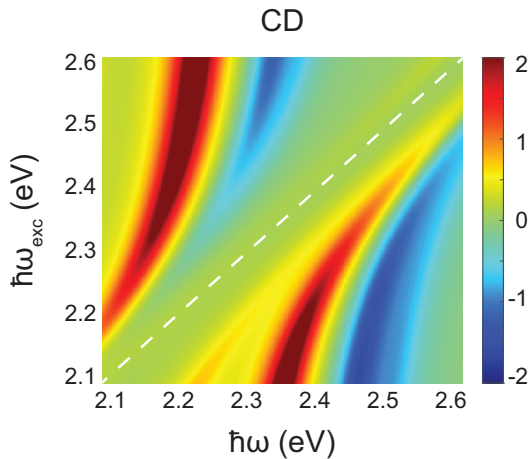


FIG. 5. Photon versus exciton energy colour map of the CD corresponding to the helix of Fig. 4.

The resulting CD spectrum is shown in Fig. 4(c), exhibiting two intense resonant features of opposite signs at around 2.3 eV and 2.4 eV, with an inflection point between them. These are exactly the CD features that we will try to manipulate through strong coupling with the excitonic layer. Fig 4(d) shows the same helix as in (a), now embedded in the matrix described above. Depending on its energy, the excitonic transition of the matrix interacts more strongly with one of the two helix resonances, leading to its splitting into two peaks. This is shown for example in Fig. 4(e), for the excitonic transition depicted in panel (b); the interaction leads to a wide anticrossing between peaks B_1 and B_2 , of the order of 300 meV. Interestingly, because the second chain resonance, labeled as A in Fig. 4(b), is also close in energy, it can also couple to the exciton; at the same time, the excitonic layer itself supports the geometric resonance C [48] that still manifests as an uncoupled spectral feature at 2.4 eV. As a consequence, the absorption spectrum is now characterized by five resonances, each with different chirality properties. Tracing which of the split branches corresponds to which original resonance is straightforward, as

the hybrid modes still maintain the preference in handedness of the uncoupled ones: in this particular example, the resonances with higher amplitude under RCP incidence (A_1 , A_2) originate from resonance A, while higher LCP intensity (B_1 , B_2) corresponds to resonance B. Since resonance C is entirely related to the matrix, it has no handedness and its CD signal is practically zero, as one can see in Fig. 4(f). Comparing Figs. 4(c) and (f), one can argue that the introduction of the excitonic matrix has led to a reduction of the maximum measured CD signal over the energy window of interest. In principle, this could be intuitively anticipated, since the contribution of an achiral absorbing medium has been added to the total absorption cross sections of eqn (4a). However, the splitting of the resonant features and the manifestation of new peaks itself, in a way enhances the CD signal, since high values are measured at energies where, otherwise, the uncoupled structure would give zero. Indeed, in Figs. 4(c) and (f) energy windows of overall enhancement of the chiral response can be identified, e.g. at about 2.2 eV, where the valley of nearly zero CD in the uncoupled case [Fig. 4(c)] becomes a resonance in the case of the coupled system [Fig. 4(f)] exactly due to the hybridization and the emergence of new absorption resonances and their corresponding features in CD.

By allowing ω_{exc} to vary, one can scan the entire energy window of interest, and obtain the CD colour map of Fig. 5. Here it is more evident how the one band of strong CD shown in Fig. 4(c) has transformed into two, separated by an anticrossing with practically zero CD, following the linear dispersion corresponding to the exciton-polariton resonance of the matrix itself. It is also clear that, due to this hybridization, one can tune the system so as to exhibit strong optical chirality at energies up to 0.2 eV away from the corresponding window in the uncoupled case, thus enabling the post-manufacturing manipulation of the chirality of a structurally chiral object. Finally, it should be noted that similar CD maps are obtained for other directions of light propagation as well (albeit shifted somehow in energy —longer chains are, in this respect more preferable, since their response tends to be more isotropic [53]), meaning that the effect should be visible even in the case of an ensemble of such helices immersed in a resonant solution.

III. CONCLUSIONS

We theoretically explored the possibility of manipulating the chiroptical response of two distinct nanostructures, with different types of chirality, through coupling with excitonic materials. The chirality density of a field is correlated to overlapping parallel electric and magnetic field components. These components become reconfigurable upon addition of the excitonic material, which then translates into a reconfigurable signal in the scattering and absorption properties of the chiral structure, such as DS and CD. The effect is most evident when

the system operates closer to the strong coupling regime, where the properties of each component are tied together and the coupled configuration is characterized by hybrid light-matter resonances. We demonstrated that the introduction of excitonic components can lead to the amplification of the intensity of the measured signal, or to the emergence of new spectral features that inherit the handedness of the uncoupled structure. As a practical example, we focused on plasmonic spheres in a helical arrangement; nevertheless, our findings can be directly extended to any other system exhibiting natural, structural, or magnetic chirality.

AUTHOR CONTRIBUTIONS

C. T., P. E. S., and S. D. conceived the idea. P. E. S. performed the calculations on the single nanoparticle. C. T. performed the calculations on the nanoparticle helix. All authors contributed equally to the discussion of

the results and the writing of the paper.

CONFLICTS OF INTEREST

There are no conflicts to declare.

ACKNOWLEDGEMENTS

P. E. S. is the recipient of the Zonta Denmark's Scholarship for female PhD students in Science and Technology 2021. N. A. M. is a VILLUM Investigator supported by VILLUM FONDEN (Grant No. 16498). G. P. A. acknowledges support from the Swiss National Science Foundation (200021_184687) and National Center of Competence in Research Bio-Inspired Materials NCCR (51NF40_182881).

-
- [1] M. Sun, T. Hao, X. Li, A. Qu, L. Xu, C. Hao, C. Xu, and H. Kuang, *Nat. Commun.* **9**, 4494 (2018).
- [2] L. A. Nguyen, H. He, and C. Pham-Huy, *Int. J. Biomed. Sci.* **2**, 85 (2006).
- [3] G. Alvarez-Rivera, M. Bueno, D. Ballesteros-Vivas, and A. Cifuentes, *Trends Anal. Chem.* **123**, 115761 (2020).
- [4] N. Berova, K. Nakanishi, and R. W. Woody, eds., *Circular Dichroism: Principles and Applications, 2nd Ed.* (John Wiley and Sons, New York, 2000).
- [5] M. Hentschel, M. Schäferling, X. Duan, H. Giessen, and N. Liu, *Sci. Adv.* **3**, e1602735 (2017).
- [6] E. Petronijevic, A. Belardini, G. Leahu, R. Li Voti, and C. Sibilìa, *Opt. Mater. Express* **12**, 2724 (2022).
- [7] J. T. Collins, C. Kuppe, D. C. Hooper, C. Sibilìa, M. Centini, and V. K. Valev, *Adv. Opt. Mater.* **5**, 1700182 (2017).
- [8] E. Plum, J. Zhou, J. Dong, V. A. Fedotov, T. Koschny, C. M. Soukoulis, and N. I. Zheludev, *Phys. Rev. B* **79**, 035407 (2009).
- [9] J. K. Gansel, M. Thiel, M. S. Rill, M. Decker, K. Bade, V. Saile, G. von Freymann, S. Linden, and M. Wegener, *Science* **325**, 1513 (2009).
- [10] P. Lodahl, S. Mahmoodian, S. Stobbe, A. Rauschenbeutel, P. Schneeweiss, J. Volz, H. Pichler, and P. Zoller, *Nature* **541**, 473 (2017).
- [11] C. D. Aiello, J. M. Abendroth, M. Abbas, A. Afanasev, S. Agarwal, A. S. Banerjee, D. N. Beratan, J. N. Belling, B. Berche, A. Botana, J. R. Caram, G. L. Celardo, G. Cuniberti, A. Garcia-Etxarri, A. Dianat, I. Diez-Perez, Y. Guo, R. Gutierrez, C. Herrmann, J. Hihath, S. Kale, P. Kurian, Y.-C. Lai, T. Liu, A. Lopez, E. Medina, V. Mujica, R. Naaman, M. Noormandipour, J. L. Palma, Y. Paltiel, W. Petuskey, J. C. Ribeiro-Silva, J. J. Saenz, E. J. G. Santos, M. Solyanik-Gorgone, V. J. Sorger, D. M. Stemer, J. M. Ugalde, A. Valdes-Curiel, S. Varela, D. H. Waldeck, M. R. Wasielewski, P. S. Weiss, H. Zacharias, and Q. H. Wang, *ACS Nano* **16**, 4989 (2022).
- [12] I. Dolamic, S. Knoppe, A. Dass, and T. Bürgi, *Nat. Commun.* **3**, 798 (2012).
- [13] X. Lan, X. Lu, C. Shen, Y. Ke, W. Ni, and Q. Wang, *J. Am. Chem. Soc.* **137**, 457 (2015).
- [14] S. Droulias, *Phys. Rev. B* **102**, 075119 (2020).
- [15] N. Maccaferri, I. Zubritskaya, I. Razdolski, I.-A. Chioar, V. Belotelov, V. Kapaklis, P. M. Oppeneer, and A. Dmitriev, *J. Appl. Phys.* **127**, 080903 (2020).
- [16] J. M. Caridad, C. Tserkezis, J. E. Santos, P. Plochocka, M. Venkatesan, J. M. D. Coey, N. A. Mortensen, G. L. J. A. Rikken, and V. Krstić, *Phys. Rev. Lett.* **126**, 177401 (2021).
- [17] P. E. Stamatopoulou, V. Yannopoulos, N. A. Mortensen, and C. Tserkezis, *Phys. Rev. B* **102**, 195415 (2020).
- [18] L. D. Barron, *Molecular Light Scattering and Optical Activity* (Cambridge University Press, Cambridge, 2004).
- [19] L. A. Warning, A. R. MianDashti, L. A. McCarthy, Q. Zhang, C. F. Landes, and S. Link, *ACS Nano* **15**, 15538 (2021).
- [20] E. Hendry, T. Carpy, J. Johnston, M. Popland, R. V. Mikhaylovskiy, A. J. Laphorn, S. M. Kelly, L. D. Barron, N. Gadegaard, and M. Kadodwala, *Nat. Nanotechnol.* **5**, 783 (2010).
- [21] S. Droulias and L. Bougas, *Nano Lett.* **20**, 5960 (2020).
- [22] V. K. Valev, J. J. Baumberg, C. Sibilìa, and T. Verbiest, *Adv. Mater.* **25**, 2517 (2013).
- [23] X. Mu, L. Hu, Y. Cheng, Y. Fang, and M. Sun, *Nanoscale* **13**, 581 (2021).
- [24] A. García-Etxarri and J. A. Dionne, *Phys. Rev. B* **87**, 235409 (2013).
- [25] J. Lasa-Alonso, D. R. Abujetas, Á. Nodar, J. A. Dionne, J. J. Sáenz, G. Molina-Terriza, J. Aizpurua, and A. García-Etxarri, *ACS Photonics* **7**, 2978 (2020).
- [26] F. Graf, J. Feis, X. Garcia-Santiago, M. Wegener, C. Rockstuhl, and I. Fernandez-Corbaton, *ACS Photonics* **6**, 482 (2019).
- [27] A. Kuzyk, R. Schreiber, Z. Fan, G. Pardatscher, E.-M. Roller, A. Högele, F. C. Simmel, A. O. Govorov, and

- T. Liedl, *Nature* **483**, 311 (2012).
- [28] A. O. Govorov, *J. Phys. Chem. C* **115**, 7914 (2011).
- [29] B. M. Maoz, R. van der Weegen, Z. Fan, A. O. Govorov, G. Ellestad, N. Berova, E. Meijer, and G. Markovich, *J. Am. Chem. Soc.* **134**, 17807 (2012).
- [30] X. Duan, S. Yue, and N. Liu, *Nanoscale* **7**, 17237 (2015).
- [31] M. L. Solomon, J. Hu, M. Lawrence, A. García-Etxarri, and J. A. Dionne, *ACS Photonics* **6**, 43 (2018).
- [32] T. V. Raziman, R. H. Godiksen, M. A. Müller, and A. G. Curto, *ACS Photonics* **6**, 2583 (2019).
- [33] W. Zhang, T. Wu, R. Wang, and X. Zhang, *Nanoscale* **9**, 5701 (2017).
- [34] K. Yao and Y. Liu, *Nanoscale* **10**, 8779 (2018).
- [35] N. T. Fofang, T.-H. Park, O. Neumann, N. A. Mirin, P. Nordlander, and N. J. Halas, *Nano Lett.* **8**, 3481 (2008).
- [36] P. Törmä and W. L. Barnes, *Rep. Prog. Phys.* **78**, 013901 (2015).
- [37] C. Tserkezis, P. A. D. Gonçalves, C. Wolff, F. Todisco, K. Busch, and N. A. Mortensen, *Phys. Rev. B* **98**, 155439 (2018).
- [38] F. Todisco, R. Malureanu, C. Wolff, P. A. D. Gonçalves, A. S. Roberts, N. A. Mortensen, and C. Tserkezis, *Nanophotonics* **9**, 803 (2020).
- [39] G. W. Castellanos, S. Murai, T. V. Raziman, S. Wang, M. Ramezani, A. G. Curto, and J. Gómez Rivas, *ACS Photonics* **7**, 1226 (2020).
- [40] F. Wu, J. Guo, Y. Huang, K. Liang, L. Jin, J. Li, X. Deng, R. Jiao, Y. Liu, J. Zhang, W. Zhang, and L. Yu, *ACS Nano* **15**, 2292 (2021).
- [41] J. Zhu, F. Wu, Z. Han, Y. Shang, F. Liu, H. Yu, L. Yu, N. Li, and B. Ding, *Nano Lett.* **21**, 3573 (2021).
- [42] E. U. Condon, *Rev. Mod. Phys.* **9**, 432 (1937).
- [43] Y. Tang and A. E. Cohen, *Phys. Rev. Lett.* **104**, 163901 (2010).
- [44] I. Fernandez-Corbaton, X. Zambrana-Puyalto, N. Tischler, X. Vidal, M. L. Juan, and G. Molina-Terriza, *Phys. Rev. Lett.* **111**, 060401 (2013).
- [45] C. F. Bohren and D. R. Huffman, *Absorption and Scattering of Light by Small Particles* (John Wiley and Sons, New York, 1983).
- [46] G. Mie, *Ann. Phys.* **330**, 377 (1908).
- [47] C. Tserkezis, A. I. Fernández-Domínguez, P. A. D. Gonçalves, F. Todisco, J. D. Cox, K. Busch, N. Stenger, S. I. Bozhevolnyi, N. A. Mortensen, and C. Wolff, *Rep. Prog. Phys.* **83**, 082401 (2020).
- [48] T. J. Antosiewicz, S. P. Apell, and T. Shegai, *ACS Photonics* **1**, 454 (2014).
- [49] Z. Fan and A. O. Govorov, *J. Phys. Chem. C* **115**, 13254 (2011).
- [50] C. Song, M. G. Blaber, G. Zhao, P. Zhang, H. C. Fry, G. C. Schatz, and N. L. Rosi, *Nano Lett.* **13**, 3256 (2013).
- [51] A. Kuzyk, R. Jungmann, G. P. Acuna, and N. Liu, *ACS Photonics* **5**, 1151 (2018).
- [52] A. T. M. Yeşilyurt and J. S. Huang, *Adv. Opt. Mater.* **9**, 2100848 (2021).
- [53] C. Tserkezis, A. T. M. Yeşilyurt, J.-S. Huang, and N. A. Mortensen, *ACS Photonics* **5**, 5017 (2018).
- [54] P. B. Johnson and R. W. Christy, *Phys. Rev. B* **6**, 4370 (1972).
- [55] N. Liu and T. Liedl, *Chem. Rev.* **118**, 3032 (2018).
- [56] C. Tserkezis, R. W. Taylor, J. Beitner, R. Esteban, J. J. Baumberg, and J. Aizpurua, *Part. Part. Syst. Charact.* **31**, 152 (2014).